

## Static and Dynamic Indentation Damage in SiC and Si<sub>3</sub>N<sub>4</sub>

Jong Ho Kim<sup>1</sup>, Young-Gu Kim<sup>1</sup>, Do Kyung Kim<sup>1, a</sup>,  
Kee Sung Lee<sup>2, b</sup> and Soon Nam Chang<sup>3, c</sup>

<sup>1</sup>Department of Materials Science and Engineering Korea Advanced Institute of Science and Technology 373-1 Kusong-dong, Yusong-gu, Daejeon, 305-701, Korea

<sup>2</sup>School of Mechanical and Automotive Engineering, Kookmin Univ., Seoul, 136-702, Korea

<sup>3</sup>Agency for Defense Development, Yusong, P.O. Box 35-1, Daejeon, 305-600, Korea

<sup>a</sup>dkkim@kaist.ac.kr, <sup>b</sup>keeslee@kookmin.ac.kr, <sup>c</sup>snchang33@add.re.kr

**Keywords:** SiC, Si<sub>3</sub>N<sub>4</sub>, Indentation, Dynamic fracture, Impact damage, Quasiplasticity

**Abstract.** Hertzian and explosive indentations were used to determine the damage behavior of SiC and Si<sub>3</sub>N<sub>4</sub> ceramics. Specimens were selected with different microstructures. In order to observe the subsurface damaged zone, the bonded interface technique was adopted. It was found that the damage response depends strongly on the microstructure of ceramics. Examination of subsurface damage reveals a competition between brittle and quasiplastic damage mode: brittle fracture mode is dominant in fine grain microstructure; quasiplastic deformation occurs in coarse grain. Dynamic indentation induces subsurface yield zone which contains extensive micro-cracks. The role of microstructure on static and dynamic damage behavior are discussed in terms of the weakness of grain boundary and grain size.

### Introduction

Silicon nitride and carbide have extensively studied for structural applications due to a favorable combination of properties that include high strength, high hardness, moderate thermal conductivity, low thermal expansion coefficient, and unusual high fracture toughness.[1] These materials have been successfully demonstrated in a variety of applications, e.g., cutting tools, bearings, gas turbine engine components, and armor.[1] The understanding of mechanical properties at the microstructural level is critical for utilization and optimal design.[2] In order to investigate the microstructural effect on indentation damage behavior, Hertzian testing is preferred because it provides a tendency for brittle or quasiplastic deformation according to microstructure in brittle ceramics.[3] Several tough ceramics have been characterized with Hertzian testing method, including silicon carbide and nitride with controlled microstructure.[4] In present work, we followed the method of previous research for microstructure variation on static indentation damage.

Silicon nitride and carbide are occasionally subjected to impact loading conditions which may cause the catastrophic failure through localized damage accumulation. It is generally considered that the process occurring in dynamic deformation can differ significantly from static or quasistatic situations.[5] On the other hand, it is suggested that static mechanical properties are related to dynamic deformation.[6] However attempts to relate the static and dynamic damage are still insufficient. Preliminary studies with dynamic indentation and finite element method were conducted on typical ceramic materials.[7] We extend our investigations of static and dynamic indentation damages to cover the structural ceramics: Si<sub>3</sub>N<sub>4</sub> and SiC.

In this study, we examine static and dynamic indentation damage on SiC and Si<sub>3</sub>N<sub>4</sub> prepared by different routes. We consider two grades of silicon carbide fabricated by hot press (HP) and solid state sintering (SS) methods and three grades of silicon nitride with increasing grain size, fine equiaxed (F), medium (M), and coarse elongated (C) which most closely represent structural ceramics. The purpose of

this study is two folds: to study the effect of microstructure on dynamic indentation damage and to find the relationship between static and dynamic indentation damage.

### Processing and Preparatory Characterization of SiC and Si<sub>3</sub>N<sub>4</sub>

**a) Processing** The starting silicon nitride powder consisted of  $\alpha$ -Si<sub>3</sub>N<sub>4</sub> (UBE-SN-E10, Ube Industries, Tokyo, Japan) with following additives: 5 wt% Y<sub>2</sub>O<sub>3</sub> (Fine Grade, H. C. Starck GmbH, Goslar, Germany), 2 wt % Al<sub>2</sub>O<sub>3</sub> (AKP50, Sumitomo Chemical Co. Ltd. Tokyo, Japan), and 1 wt% MgO (High Purity Baikowski Co. NC. U.S.A.). The powders were mixed as a slurry in isopropanol for 24 hours in a planetary ball mill, using zirconia balls in a propylene container. After drying, the softly agglomerated powder was crushed and sieved through 60 mesh screen. Densification was achieved in nitrogen gas at 1 atm under uniaxial stress 25 MPa, at 1600, 1700 and 1800 °C for 1 hour in a hot press (Astro Industries Inc., CA, U.S.A.). These sintering temperature produced fine equiaxed (F), medium (M), coarse elongated (C) microstructure.

Silicon carbide samples were obtained from a commercial source (Ceradyne, CA, U.S.A.). Two grades of silicon carbide were used for these experiments: The one was fabricated through hot pressing (HP) and the other by the solid state sintering (SS) method. The consolidation process also strongly affects the microstructure and phase compositions: the HP specimen contains primarily all  $\alpha$  with a small amount of  $\beta$  phase and a glassy grain boundary layer and SS specimen contains only  $\alpha$  phase and dry grain boundaries.

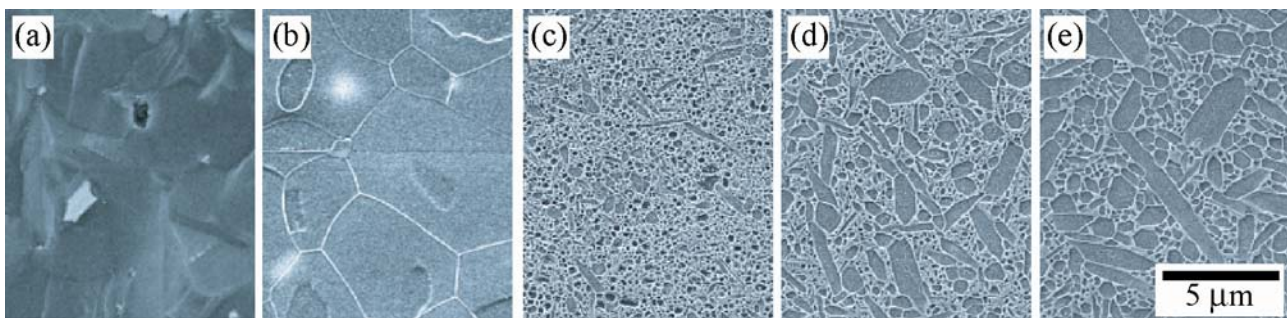


Fig. 1: SEM micrographs of specimens: (a) SS-SiC, (b) HP-SiC, (c) F-Si<sub>3</sub>N<sub>4</sub>, (d) M-Si<sub>3</sub>N<sub>4</sub>, and (e) C-Si<sub>3</sub>N<sub>4</sub>

**b) Microstructure, Strength and Toughness** Specimen surfaces normal to the hot pressing direction were polished to 1  $\mu$ m finish to enable characterization. These surfaces were plasma etched to highlight the grain structures, except SS-SiC due to difficulty of etching. The fractured surface of SS-SiC is used to reveal microstructure. The microstructures of the specimens were observed by scanning electron microscope (SEM). Figure 1 shows SEM images of specimens. HP-SiC exhibits glassy grain boundary phases and  $\sim$ 10  $\mu$ m equiaxed  $\alpha$  grains and a small amount of  $\beta$  phase. SS-SiC microstructure is not clearly shown so that the shape and size of grains were predicted by fractography. SS-SiC tends to undergo brittle fracture through transgranular crack propagation. Silicon nitrides have bimodal structures with different ratio of  $\alpha$  and  $\beta$ : F-Si<sub>3</sub>N<sub>4</sub> with  $\sim$ 75 %  $\sim$ 0.5  $\mu$ m  $\alpha$  grains and  $\sim$ 15 %  $\beta$  grains, M-Si<sub>3</sub>N<sub>4</sub> with  $\sim$ 78 %  $\sim$ 0.5  $\mu$ m wide and  $\sim$ 4  $\mu$ m long  $\beta$  grains and  $\sim$ 12 % of  $\alpha$  grains, C-Si<sub>3</sub>N<sub>4</sub> has 100 %  $\sim$ 1.5  $\mu$ m wide and  $\sim$ 9.0  $\mu$ m long  $\beta$  grains. In all specimens except SS-SiC, a weak glassy phase covers all grain boundary surfaces as an amount of  $\sim$ 10 vol%.

Silicon Carbide and Nitride Data

Material	HP-SiC	SS-SiC	F- Si <sub>3</sub> N <sub>4</sub>	M-Si <sub>3</sub> N <sub>4</sub>	C-Si <sub>3</sub> N <sub>4</sub>
Processing condition	Hot-press	Solid-state sintering	Hot-press at 1600 °C	Hot-press at 1700 °C	Hot-press at 1800 °C
Hardness, $H$ (GPa)	19.5	29.1	20.6	16.5	15.9
Toughness, $T$ (MPa m <sup>1/2</sup> )	3.75	2.46	3.8	5.3	4.9-7.3 †
Strength, $\sigma_F$ (MPa)	525	523	885	1084	792
Young's modulus, $E$ (GPa)	442	440	331	326	314
Poisson's ration, $\nu$	0.17	0.17	0.27	0.28	0.29
Yield stress, $Y$ (GPa)	8.9	9.4	11.7	9.5	7.2
Strain hardening coefficient	0.8	0.7	1	0.7	0.5

† R-curve behavior is observed

Table 1: Processing and physical properties of each material

Table 1 shows the basic physical properties of various specimens. The density of the specimen was determined by Archimedes method and it confirms that specimens are near full density. Young's modulus and Poisson's ratio were determined for each sample using routine impulse excitation technique. The Vickers indentations were used to determine the hardness of materials, using  $H=P/2a^2$ , where  $P$  is load and  $a$  is half-diagonal. In order to obtain strength, the flexure tests were conducted in four-point bending, using  $\sigma = 3P/l/2wd^2$ , where  $P$  is load,  $l$  is length between spans,  $w$  is width, and  $d$  is half thickness. Another set of bend tests was made on specimens after Vickers indentation to estimate the toughness, with simple equation  $T_0=0.62(E/H)^{1/8}(\sigma P^{1/3})^{3/4}$  where  $E$  is modulus,  $H$  is hardness,  $\sigma$  is strength, and  $P$  is load.[8]

### Static: Hertzian Indentation Damages

Hertzian indentation test were conducted to observe the evolution of damage in each specimens. The specimens were cut into 6 mm X 8 mm X 20 mm bars for testing. The top surface of specimens were ground and polished to 1  $\mu$ m diamond slurry finish. Side surfaces normal to the top surface were also polished for observation of subsurface damage. The opposing side surfaces were polished and glued together using adhesive to produce 'bonded interface' specimens.[9] After Hertzian indentation testing, these bonded interface specimens were separated and adhesive was removed by acetone. These separated side surface were gold coated for viewing in Nomarski interference optical microscope and SEM.

Specimens were subjected to top surface contact loading from a WC sphere indenter ( $r = 1.2\sim 12.7$  mm) using mechanical loading machine (Model 4400R, Instron Co. MA, U.S.A.). Indentation stress-strain curves were measured for each specimen at loads up to  $P = 5000$  N. From measurement of contact radius  $a$  at each value of  $P$  and  $r$ , indentation stress  $p_0=P/\pi a^2$ , and indentation strain  $a/r$ , could be evaluated. Indentation stress strain response of specimens can be analyzed using  $\sigma = E \epsilon$  where  $\sigma \leq Y$  and  $\sigma = Y + \alpha (\epsilon E - Y)$  where  $\sigma > Y$ . Using the previous relationships to obtain a best fit of curve, the brittle and quasiplastic regions can be separated by transition point, and the yield strength  $Y$  and strain-hardening coefficient  $\alpha$  can be determined. Estimated values for each material are listed in table 1.

Figure 2 shows subsurface damage of each specimen. Observed damage patterns are good agreements with general trends that the transition, fracture dominated to deformation dominated occurs with increasing heterogeneity of microstructure and long crack toughness. As seen in Figure 2, cone cracking is dominant in SS and F, quasiplasticity in C, and combination of cone cracking and quasiplasticity in HP and M.

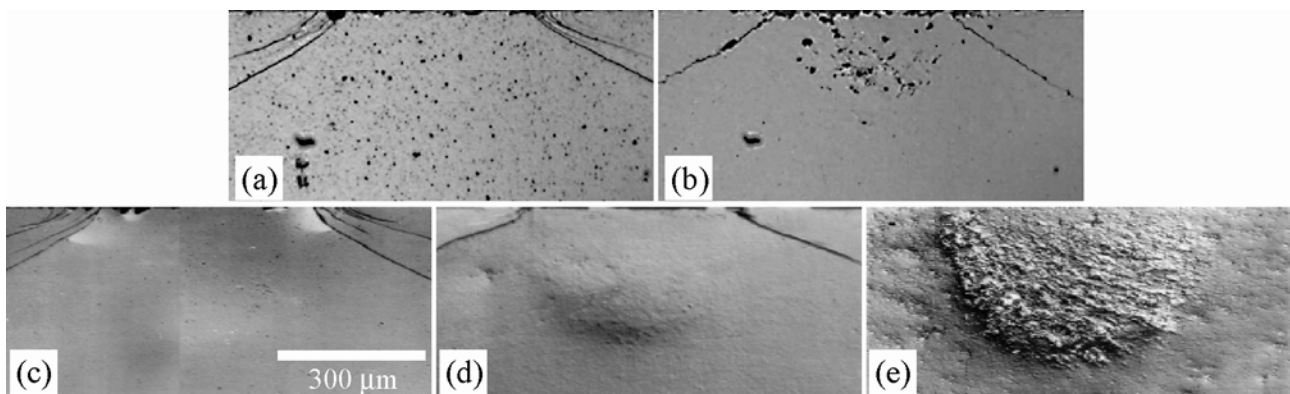


Fig. 2: Side Views of Hertzian contact damage: (a) SS-SiC, (b) HP-SiC, (c) F-Si<sub>3</sub>N<sub>4</sub>, (d) M-Si<sub>3</sub>N<sub>4</sub>, and (e) C-Si<sub>3</sub>N<sub>4</sub>. Transition from brittle to quasi-plastic damage behavior is apparently observed the SS → HP-SiC series and the F→M→C- Si<sub>3</sub>N<sub>4</sub> series.

### Dynamic: Explosive Indentation Damages

Explosive indentation testing was made on similar bonded interface specimens to reveal dynamic deformation of specimens. These specimens were clamped with auxiliary fixture to inhibit shattering of specimen during impact loading. Shock impact indentation was performed using the electric bridge wire (EBW) detonator. The small explosive detonator encased in a stainless steel (150 μm thickness) cylinder and 5 mm diameter bottom plate. This detonator propels the bottom stainless steel flyer to specimen about 1 km/s velocity to generate impact shock compression. After testing, the specimens were separated, cleaned, and observed with the optical microscopy and the SEM.

Figure 3 shows side views of explosively indented specimens. As seen in side views, radial and lateral cracks were distributed in entire region of specimen, accompanying with the fragmentation and spallation. The shock compression propagates through the specimens and the shock wave is reflected at the end of sample and interface between specimen and guide metal blocks. These macroscopic cracking and spallation events seem to represent post-shock damage because the reflected wave breaks the specimen into several pieces. This can be inferred from the fact that macroscopic cracks exist through the entire specimens and similar trends of crack pattern are seen independent on materials and microstructure. The characteristic that macro-cracks and large spallation are dominant occurs in the specimens: SS and F. The extensive failure of SS and F during impact loading is still true even though spallation happens during post-shock. These fracture behavior is considered as a structural effect related to specimen dimension and test configuration so that this damage mode can be avoided with proper impedance match design.

A particular characteristic of shock compression deformation is quasiplastic damage mode in the specimens: HP, M, and C. The distinctive deformation dominant damage pattern is pronounced as the quasiplastic damage prevails in Hertzian testing for HP, M, and C specimen. Shear faults or micro-fractures play an important role in quasiplastic deformation in Hertzian indentation damages and these criteria coincides with the damage behavior in dynamic indentation. The quasiplastic damage zone can be described properly as a cloud of many localized micro-cracks. In the HP specimen, the quasi-plastic damage zone is strongly distinguished from the far shock indented region, compared with the other materials. For silicon nitride specimens, quasiplastic deformation zone area is increased with increasing amount of  $\beta$  elongated grain through the sequence F→M→C, but the area is smaller than that of SiC.



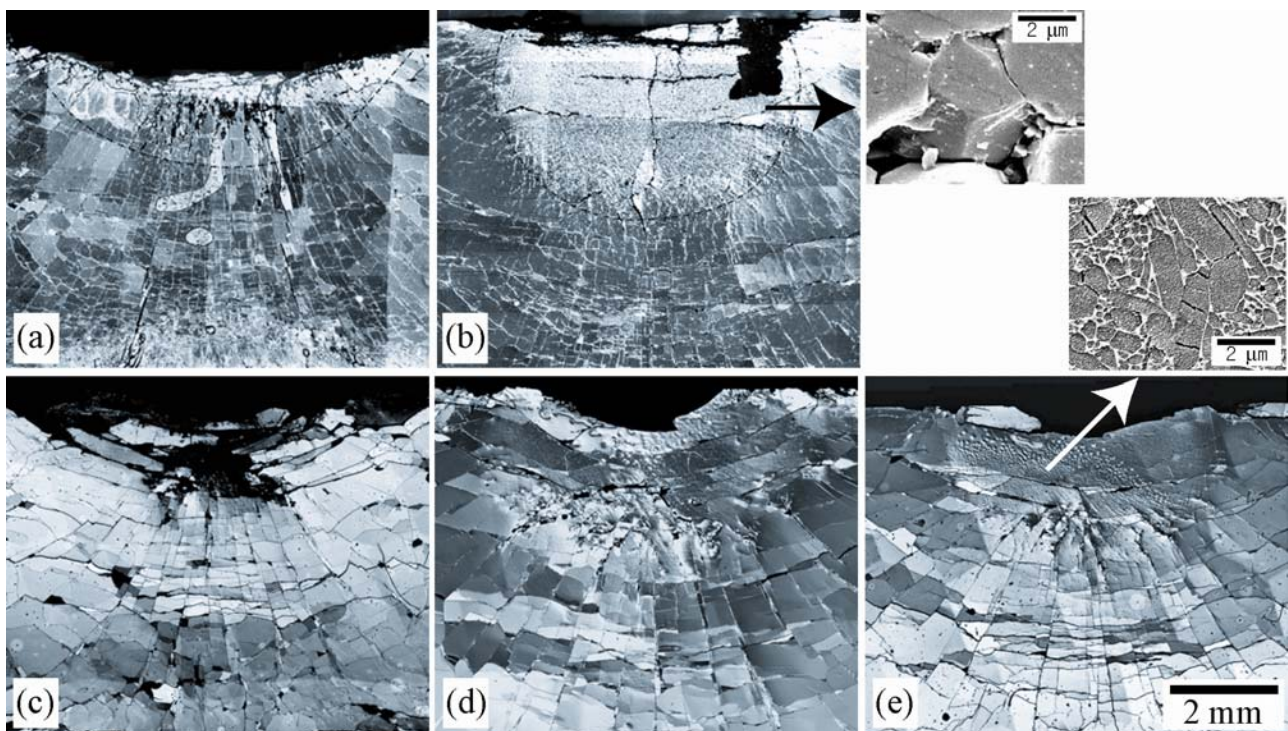


Fig. 3: Side Views of explosive indentation damage: (a) SS-SiC, (b) HP-SiC, (c) F-Si<sub>3</sub>N<sub>4</sub>, (d) M-Si<sub>3</sub>N<sub>4</sub>, and (e) C-Si<sub>3</sub>N<sub>4</sub>. Massive quasi-plasticity damage zone was apparently created in the specimen: HP and C, partially in M.

### Discussion

We have characterized the dynamic indentation damage mode in silicon carbide and nitride in term of fabrication process and microstructure. Consider two grades of silicon carbide with different microstructure: HP-SiC contains thin glassy phase in grain boundary and SS-SiC grain boundary with no glassy phase. These microstructural differences cause quasiplastic and brittle damage modes. During dynamic compression, the weak glassy grain boundary tends to fail, and this is the reason why HP-SiC shows ductile and SS-SiC brittle failure. Defeating weak grain boundary was also mentioned in Shih et. al. and Lundberg et. al.'s preceding studies.[10, 11] In the Figure 3, upper right two micrographs, quasiplastic deformation zone was observed in high magnification. Intergranular fracture seen in micrographs proves that shear faults are main damage mode in quasiplastic deformed zone.

In case of silicon nitride, all specimens contain almost the same amount of weak glassy phase in grain boundary. However these three grades of silicon nitride exhibit a transition from fracture dominated to quasiplasticity dominated damage with variation of microstructure. In Hertzian indentation of Lee et. al.'s work [4], this trend was explained with microstructural heterogeneity associated with the amount of elongated  $\beta$  grain. This explanation can be applied to the results of our explosive indentation experiments. For the silicon carbide, a glassy grain boundary phase affords explanation of massive quasiplastic damage in HP-SiC. Contrary to silicon carbide, silicon nitride has a relatively smaller grain size, and this affects the formation of shear faults, which results in a relatively smaller area of quasiplastic deformation zone. The elongated  $\beta$  grains in silicon nitride are relatively larger than the equiaxed grains and more likely to induce micro-failures inside the microstructure. The combination of grain boundary structure and grain influence the transition from brittle to ductile failure in the structural ceramics. The

grain boundary structure and grain size are possibly key factors in the shock compression deformation in silicon nitride and carbide ceramics.

The results of this study provide a basic consideration for the application of ceramic armor materials. In the ballistic testing of armor ceramics, massive damage was observed where shock compression is concentrated. By comparison of our result to previous ballistic testing on ceramics, we suspect that quasiplastic deformation is analogous to massive shock front damage before the projectile penetrates into ceramics. Dynamic indentation test would thus appear to provide a useful evaluation of armor ceramics. It is of interest to compare the Hertzian indentation and explosive indentation damage in terms of brittle fracture and ductile deformation. In order to observe quasiplasticity, Hertzian indentation shows pronounced effects in silicon nitride and explosive indentation in silicon carbide. It is worth noting that these two testing methods lie in same trends in indentation damage mode. We suggest that Hertzian indentation test can provide an indication of dynamic indentation damage behavior.

### Conclusion

Hertzian and explosive indentations were used to evaluate the damage behavior SiC and Si<sub>3</sub>N<sub>4</sub> ceramics. The microstructural differences of silicon carbide (i.e., absence or existence of glassy phase at grain boundary) cause a transition from brittle to quasiplastic damage modes. In the case of silicon nitride, the transition from fracture dominated to quasiplasticity dominated damage is associated with variation of microstructure. Grain boundary structure and grain size are key factors for determination of brittle or ductile failure in structural ceramics. In addition, Hertzian indentation test is suggested as a mean to assess dynamic indentation damage of ceramics.

### References

- [1] David W. Richerson, Douglas W. Freitag, Technical Report DOE/ORO 2076. (1998), pp 2.125.
- [2] P. F. Becher, S. L. Hwang, H. T. Lin, T. N. Tiegs, (Kluwer Academic Publishers 1994).
- [3] B. R. Lawn, J. Am. Ceram. Soc., Vol. 81, No. 8, (1998) pp. 1977.
- [4] S. K. Lee, K. S. Lee, B. R. Lawn, and D. K. Kim, J. Am. Ceram. Soc., Vol. 81, No. 8, (1998), pp. 2061.
- [5] Marc A. Meyers, *Dynamic Behavior of Materials*, (A WileyInterscience Publication 1994).
- [6] D. K. Kim, C.S. Lee, Y. G. Kim, C. W. Kim, S. N. Chang, *Ceramic Transactions: Ceramic Armor Materials by Design 2002*, pp. 261.
- [7] D. K. Kim, J. H. Kim, Y. G. Kim, C.S. Lee, D.T. Chung, C. W. Kim, J. H. Choi, S.N. Chang, *Ceramics Transactions: Ceramic Armor and Armor Systems 2003*, pp. 93.
- [8] B. R. Lawn, *Fracture of Brittle Solids Second Edition*, (Cambridge University Press 1993).
- [9] F. Guiberteau, N. P. Padture, B. R. Lawn, J. Am. Ceram. Soc., Vol. 77, No. 7, (1994)
- [10] C. J. Shih, M. A. Meyers, V. F. Nestrenko, S. J. Chen, , *Acta Materialia*, Vol. 48, (2000), pp. 2399.
- [11] P. Lundberg, R. Renstrom, B. Lundberg, *Int. J. Impact Eng.*, Vol. 24, (2000), pp.

